Journal of Applied Polymer Science

Hierarchically Porous Graphitic Carbon Monoliths Containing Nickel Nanoparticles as Magnetically Separable Adsorbents for Dyes

Yurong Liu,[1,2] Baoping Lin,[1] Dan Li,[1] Xueqin Zhang,[1] Ying Sun,[1] Hong Yang[1]

[1]School of Chemistry and Chemical Engineering, Southeast University, Nanjing 211189, People's Republic of China

[2]Chongqing Key Laboratory of Micro/Nano Materials Engineering and Technology, Research Center for Material Interdisciplinary Science, Chongqing University of Arts and Science, Chongqing 402160, People's Republic of China

Correspondence to: B. Lin (E-mail: lbp@seu.edu.cn) and Y. Liu (E-mail: liuyr8827@163.com)

ABSTRACT: The hierarchically porous graphitic carbon monoliths containing nickel nanoparticles (HPGCM-Ni) were fabricated via multi-component co-assembly in polyurethane (PU) foam scaffold associated with a direct carbonization process from triblock copolymer F127, diblock copolymer PDMS-PEO, phenolic resol, and nickel nitrate and subsequent silicates removal with NaOH solution. The decomposable PU foam scaffold played important role in the process of multi-component co-assembly and macrostructure formation. The nickel salts were reduced to metallic Ni nanoparticles during the carbonization process. The obtained HPGCM-Ni materials exhibited macropores of 100–450 μm, mesopore size of 7.2 nm, BET surface area of 725 $m^2\ g^{-1}$, pore volume of 0.74 $cm^3\ g^{-1}$, and saturation magnetization of 2.3 emu g^{-1}. Using methyl orange as model dye pollutant in water, HPGCM-Ni samples showed good adsorption capacity of 440 mg g^{-1}, exhibiting excellent adsorption characteristics desirable for the application in adsorption of dyes and separation under an external magnetic field. © 2014 Wiley Periodicals, Inc. J. Appl. Polym. Sci. **2015**, *132*, 41322.

KEYWORDS: adsorption; porous materials; self-assembly; separation techniques

Received 6 June 2014; accepted 21 July 2014

DOI: 10.1002/app.41322

INTRODUCTION

With the development of industry and technology, water pollution caused by dyes is one of the most serious problems facing mankind today. Carbon materials, such as activated carbon and mesoporous carbon are effective adsorbents for dyes because of their large specific surface area, abundant micropores and a series of surface functional groups.[1–4] However, it is difficult to separate them from the liquid medium because of their small particle sizes. The conventional separation approach normally involves filtration or centrifugation procedure, which is rather complex and expensive. At present, magnetic separation as a promising strategy has been paid more and more attention due to the fact that it can be easily separated under an applied magnetic field. Therefore, incorporation of magnetic nanoparticles into carbon matrixes has been attempted to obtain magnetically-separable porous carbons.[5–7] Nevertheless, the use of these common carbon materials on a large scale is limited by the high dispersion of active carbon powder, the amorphous pore wall, low adsorption capacity and affinity for dyes.

Hierarchical porous carbon monoliths (HPCMs) containing interconnected multi-level pores have enhanced adsorption performance compared with single-sized pore materials due to the increased mass transport through macropores and high surface area generated by meso-/micropores.[8,9] In addition, the use of monoliths as industrial adsorbents has wide operation flexibility compared to their powder counterparts.[10] Generally, HPCMs are fabricated through nanocasting pathway, which requires multiple steps and the use of pre-formed hard templates, normally porous polymer or silica monoliths.[11,12] Obviously, such strategies are rather tedious, laborious and expensive, thus limiting their production on a large scale. Other easier alternative method, such as self-assembly approach has also been used to prepare HPCMs. For example, the HPCMs have been fabricated by using commercial PU foam as sacrificial template,[13,14] which is a simple and economic pathway for the mass production of HPCMs. However, these carbon monoliths usually have amorphous carbon frameworks, which is an obvious drawback that limits their applications. In addition, these studies are rather preliminary and the applications of these monoliths unfortunately have not been explored.

Although some works have been performed in the development of HPCMs, few attentions have ever been directed towards the synthesis and applications of hierarchically porous graphitic carbon monoliths (HPGCMs).[15–17] From the viewpoint of applications, graphitic carbon has some advantages over traditional amorphous carbon, for example, the well-developed crystalline structure, intensive interaction of graphitic basic plane with organic dye molecular, good chemical, and thermal stability.[18,19]

However, until now no fabrication of magnetically separable HPGCMs has been attempted, only few reports regarding carbon powder materials of this type.[20,21]

In the present work, the HPGCMs containing magnetic nickel nanoparticles (HPGCM-Ni) have been successfully synthesized by using commercial PU foam as macroporous scaffold associated with a direct carbonization process from triblock copolymer F127, diblock copolymer PDMS-PEO, phenolic resol, and $Ni(NO_3)_2{\cdot}6H_2O$ and subsequent silicates removal with NaOH solution. The decomposable PU foam plays important role in the process of multi-component co-assembly and macrostructure formation. The nickel salts are spontaneously reduced to metallic Ni nanoparticles during the carbonization process. The obtained samples show evidently improved adsorption properties for dyes and permit an easy separation procedure. To the best of our knowledge, this kind of magnetically separable HPGCMs has not been reported before. This simple and facile fabrication method can facilitate the large-scale production of magnetically separable HPGCMs and expand their applications in the fields of adsorption and separation.

EXPERIMENTAL

Materials

PU foam with the density of 0.014 g cm^{-3} was purchased from Nanjing Chunhua Xinfei Sponge Factory. Poly(ethylene oxide)-block-poly(propylene oxide)-block- poly-(ethylene oxide) triblock copolymer Pluronic F127 ($M_w = 12{,}600$, $PEO_{106}PPO_{70}$-PEO_{106}) was purchased from Acros Corp. Polydimethylsiloxane-poly(ethylene oxide) (PDMS-PEO, $M_w = 3012$, DMS_{32}-EO_{20}) diblock copolymer was purchased from Shenzhen Meryer Chemical Technology. Other chemicals were purchased from Chongqing Chemical Corp. All chemicals were used as received without any further purification.

Synthesis of HPGCM-Ni

The resol precursor ($M_w < 500$) was prepared according to the literature,[22] except tetrahydrofuran (THF) was used as the solvent. The PU foam slab with a total volume of 10 cm^3 (4.5 × 1.5 × 1.5 cm) was first cleaned with distilled water and dried in air at 100°C for 6 h. HPGCM-Ni was prepared through the multi-component co-assembly of F127, PDMS-PEO, resol, and nickel nitrate, followed by carbonization and silicates removal. In a typical preparation, 0.75 g of F127 and 1.25 g of PDMS-PEO were dissolved in 20.0 g of THF and stirred for 10 min at 40°C to afford a clear solution. Next, 0.25 g of $Ni(NO_3)_2{\cdot}6H_2O$ and 5.0 g of 20 wt % resols' THF solution was added in sequence. After being stirred for 0.5 h, the solution was coated onto the PU foam. It took 5–8 h at room temperature to evaporate THF. Then the coated PU foam was thermocured in an oven at 100°C and 150°C for 24 h each. The product, denoted as HPGCM-Ni-as made, was pyrolyzed at 900°C for 2 h with a ramping rate of 1°C min^{-1} below 600°C and 5°C min^{-1} above 600°C. The silicate component was removed by using 1.0*M* NaOH solution. The obtained sample was denoted as HPGCM-Ni-900, where 900 was the pyrolysis temperature. As a comparison, the HPCM was also synthesized by similar approach without adding of $Ni(NO_3)_2{\cdot}6H_2O$.

Characterization

Small-angle X-ray scattering (SAXS) measurements were taken on a Nanostar U small-angle X-ray scattering system (Bruker, Germany) using Cu K_α radiation (40 kV, 35 mA). X-ray diffraction (XRD) patterns were collected on Bruker D8 Advance X-ray diffractometer using Cu K_α radiation (40 kV, 200 mA). Raman spectra were obtained with a Renishaw in Via Raman spectrometer (England), using a He-Ne laser with an excitation wavelength of 532 nm. Scanning electron microscopy (SEM) images were collected with a Hitachi S-3400N electron microscope operated at 20 kV. Transmission electron microscopy (TEM) experiments were conducted on a JEOL 2011 microscope (Japan) operated at 200 kV. N_2 adsorption-desorption isotherms were obtained using a Tristar-3020 surface area analyzer. The specific surface areas were estimated by the BET method. The Ni contents were determined by OPTIMA5300DV inductively coupled plasma-atomic emission spectrometry (ICP-AES, PE, America). Magnetic properties were measured using a VSM 7400 vibrating sample magnetometer (VSM) (Lake Shore) with a maximum applied continuous field of 18,000 G at room temperature.

Dye Adsorption Experiment

In order to investigate the adsorption properties of HPGCM-Ni-900 for dyes, methyl orange (MO) was selected as representative organic dye molecule. For typical dye adsorption measurement, 40 mg of HPGCM-Ni-900 was dispersed in 100 mL of MO solution followed by stirring at room temperature for 5, 10, 20, 30, 60, 120, 180, 360, and 720 min, respectively. The concentrations of MO were in the range 10–100 mg L^{-1}. After adsorption, the adsorbent was removed by a magnet and the dye concentration in the clear supernatant was determined by a UV-2450 Ultraviolet–visible spectrophotometer at 465 nm. The adsorbed amount of MO onto the samples was determined according to the change of concentration before and after adsorption.

RESULTS AND DISCUSSION

Morphology and Macroporous Structure

The coated PU foam has the same volume as the PU foam scaffold [Figure 1(a)]. Morphologies of HPGCM-Ni-900 have been faithfully replicated from the PU foam scaffold after carbonization [Figure 1(b)]. HPGCM-Ni-900 shows about 55% volume shrinkage and 33% linear shrinkage, but still preserves the macrostructure morphology, which is also indicative of the good thermal stability of the macroporous architecture.

The three-dimensionally (3-D) interconnecting network of PU foam scaffold has been revealed by SEM measurement. The macropore sizes of PU foam are in the range 200–500 μm [Figure 2(a)]. Its controllable interconnected skeleton macrostructure and large voids are ideal interfaces for self-assembly. SEM image of HPGCM-Ni-900 shows its 3-D macrostructure exactly replicates the skeleton of PU foam scaffold [Figure 2(b)], indicating the interconnecting macropores are well retained after calcination at 900°C. The macropore sizes evolved into the range 100–450 μm, due to the uniform framework shrinkage during the calcination process.

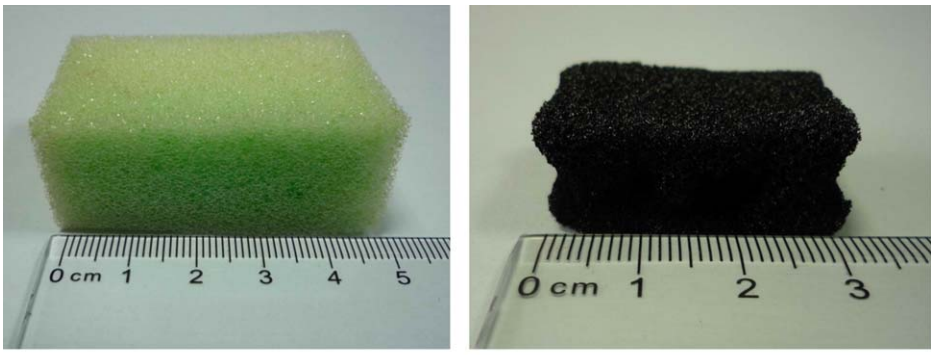

Figure 1. Photographs of (a) the coated PU foam and (b) HPGCM-Ni-900. [Color figure can be viewed in the online issue, which is available at wileyonlinelibrary.com.]

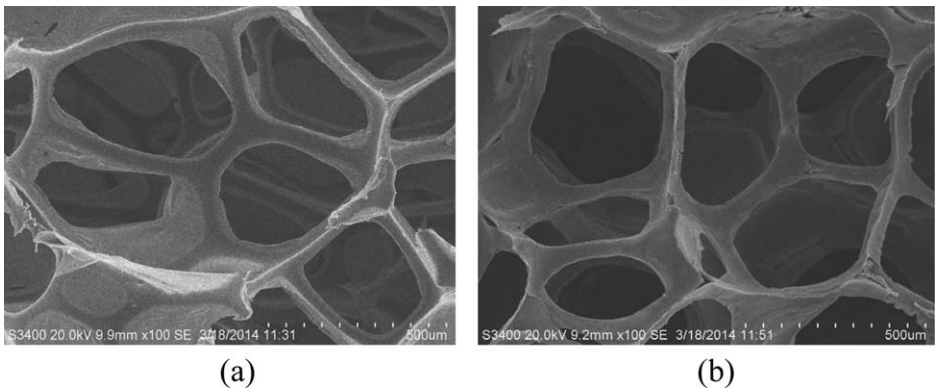

Figure 2. SEM images of (a) PU foam scaffold and (b) HPGCM-Ni-900.

Mesoporous and Graphitic Structure

SAXS patterns of as made samples [Figure 3(a,c)] show three diffraction peaks with the q value ratios $1 : \sqrt{3} : \sqrt{7}$. These diffraction peaks are indexed as 10, 11, and 21 reflections of two-dimensionally (2-D) hexagonal symmetry with the space group of *p6m*.[23] After pyrolysis at 900°C in N_2, the 10 and 11 reflections can still be observed in SAXS patterns of HPCM-900 [Figure 3(c)] and HPGCM-Ni-900 [Figure 3(d)], indicating the ordered 2-D hexagonal mesostructures are well retained. But the intensity of the reflection peaks is a little weakened and the q vectors move to higher values, implying a contraction of the framework. The unit cell parameter of HPCM is reduced from 16.1 nm to 11.7 nm upon calcination, reflecting 27% framework shrinkage. In contrast, the unit cell parameter of HPGCM-Ni is reduced from 16.5 nm to 12.5 nm, reflecting 24% framework shrinkage. This demonstrates that the presence of nickel in the carbon matrix can reduce framework shrinkage to some extent as compared to pure carbon materials (HPCM).

Wide-angle XRD patterns [Figure 4(a)] of HPCM-900 exhibit two broad diffraction peaks at 22° and 44°, corresponding to (002) and (001) diffractions of amorphous carbon, respectively.[24] Three sharp peaks at 44.5°, 51.8°, and 76.4° assigned to the (111), (200), and (220) reflection planes of face centered cubic (fcc) nickel (JCPDS card No. 040850) can be observed in XRD patterns of HPGCM-Ni-900 [Figure 4(b)], and no nickel oxide phases have been detected, indicating that Ni^{2+} has been completely reduced to metallic Ni. The size of Ni nanoparticles estimated by Scherrer equation is 20.2 nm. In addition, an intensive diffraction peak at $2\theta = 26.2°$ can be seen in Figure 4(b), which can be indexed to the (002) diffraction peak of typical graphite-like carbon, suggesting the carbon materials are well graphitized by Ni nanoparticles during carbonization process. It is well known that nanosized transitional metals favor

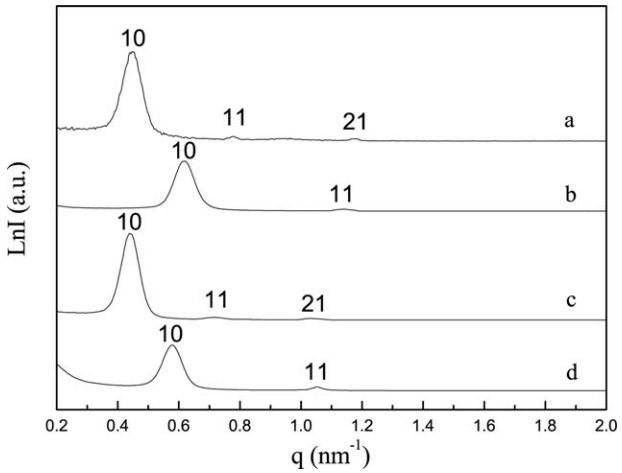

Figure 3. SAXS patterns of (a) HPCM-as made, (b) HPCM-900, (c) HPGCM-Ni-as made, and (d) HPGCM-Ni-900.

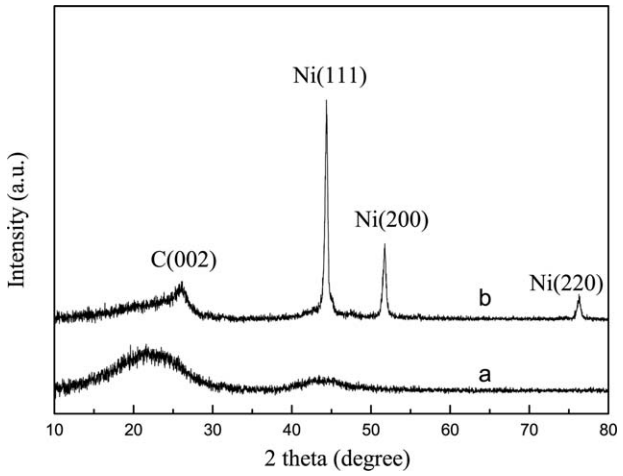

Figure 4. XRD patterns of (a) HPCM-900 and (b) HPGCM-Ni-900.

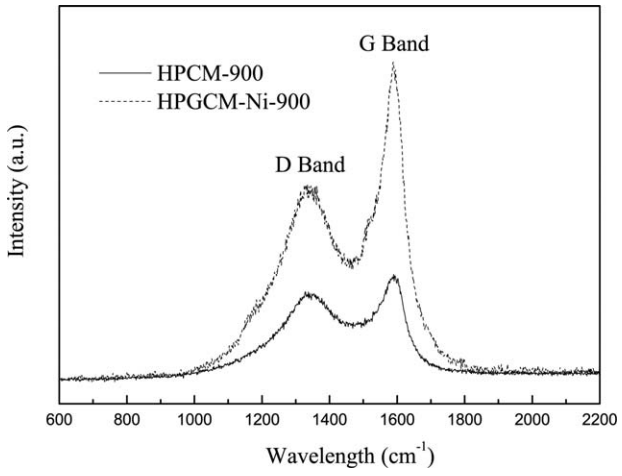

Figure 5. Raman spectra of HPCM-900 and HPGCM-Ni-900.

the formation of graphitic carbon structure when they are treated together with carbon materials at high temperatures under inert gas atmosphere.[25,26]

To further study the graphitization degree of as-prepared carbon materials, the samples have been characterized by Raman spectroscopy. A distinct pair of broad peaks at 1588 cm^{-1} and 1334 cm^{-1} can be observed in Figure 5. The vibration at 1588 cm^{-1} (G band) is associated with sp^2 hybridized carbon atoms of graphite sheets. The other peak at 1334 cm^{-1} (D band) is usually referred to the vibrations of sp^3 hybridized carbon atoms of disordered graphite.[27] The relative intensity of G and D lines (I_G/I_D) is considered to be proportional to the graphitization degree of carbon materials.[28] The I_G/I_D value of HPCM-900 is about 1.1, verifying the low degree of graphitization. By contrast, the I_G/I_D value of HPGCM-Ni-900 is 1.5, implying that HPGCM-Ni-900 materials are mainly composed of well-crystallized graphitic carbon. The detailed graphitic structures of HPGCM-Ni-900 are further detected by high resolution transmission electron microscope (HRTEM).

Figure 6 shows the typical TEM and corresponding HRTEM image of HPGCM-Ni-900. The parallel bands-like pore channels are observed in Figure 6(a), giving evidence for the presence of ordered mesoporous structure in HPGCM-Ni-900. Ni nanoparticles with the diameter of about 20–25 nm are uniformly dispersed in carbon matrix by taking advantage of confinement effect of mesoporous structure. Mesoporous carbon materials not only stabilize Ni nanoparticles by avoiding their aggregation to some extent, but also confine the growth of Ni nanoparticles. So in this way, well-dispersed and homogeneous metallic Ni nanoparticles can be incorporated into carbon matrix. The interlayer distance of graphitized carbon is estimated to be 0.34 nm [Figure 6(b)], corresponding to an interplanar spacing of graphite (002) crystal plane, indicating a remarkable improvement of graphitization degree of carbon materials resulting from in situ catalytic graphitization of amorphous carbon by Ni nanoparticles.

The pore structure of carbon materials was further studied using N_2 adsorption/desorption technique (Figure 7). The N_2 sorption isotherms of HPCM-900 and HPGCM-Ni-900 exhibit type-IV curves with clear H_1-type hysteresis loops [Figure 7(a)], indicating the well-ordered cylinder mesopore channels.[29] Figure 7(b) shows the pore-size distribution curves derived from BJH method using adsorption branches. The pore size distribution curves of HPCM-900 and HPGCM-Ni-900 display a sharp peak at 7.1 nm and 7.2 nm, respectively [Figure 7(a)]. The total pore volume of HPGCM-Ni-900 is 0.74 $cm^3\ g^{-1}$, which is larger than that of HPCM-900 (0.69 $cm^3\ g^{-1}$). However, the BET surface area of HPGCM-Ni-900 (725 $m^2\ g^{-1}$) is lower than that of

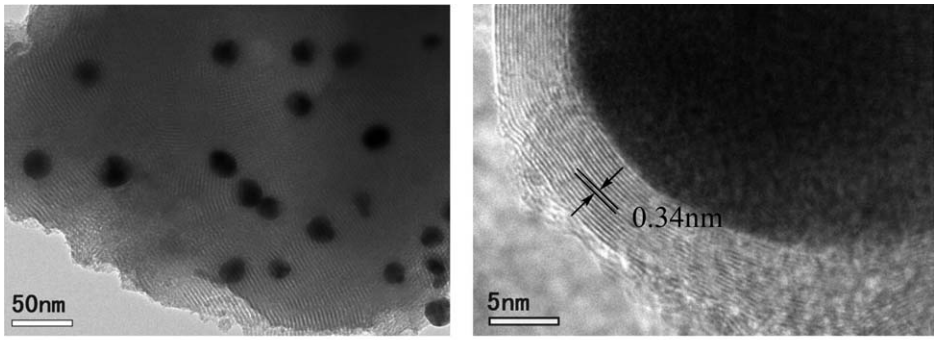

Figure 6. Typical TEM (a) and HRTEM image (b) of HPGCM-Ni-900.

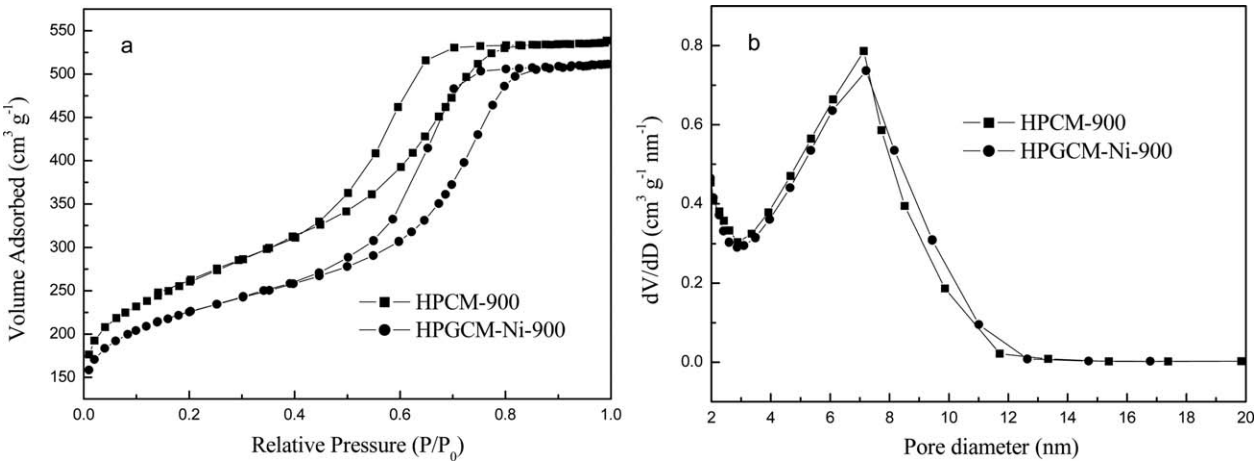

Figure 7. N_2 sorption isotherms (a) and pore size distribution curves (b) of HPCM-900 and HPGCM-Ni-900.

HPCM-900 (788 m^2 g^{-1}) due to the increased mass as a result of incorporating Ni nanoparticles.

Adsorption Performance

Figure 8 shows the adsorption of MO by HPGCM-Ni-900 as a function of contact time. It can be seen that the adsorption of MO on the carbon adsorbents is rapid at the beginning. After 10 min of reaction time, the removal efficiencies of MO at initial concentrations of 20, 50, 100, and 200 mg L^{-1} are 94%, 88%, 60%, and 54%, respectively, indicating the excellent adsorption performance of HPGCM-Ni-900 for organic dyes. After incubation of 3 h, a nearly complete removal efficiency of MO is achieved, and the adsorption equilibrium is established. HPGCM-Ni-900 has the largest adsorption amount for 200 mg L^{-1} MO, which is as high as 440 mg g^{-1}.

Separation Properties

The magnetic behaviors of HPGCM-Ni-900 have been measured by VSM at room temperature. The saturation magnetization is found to be 2.3 emu g^{-1} (Figure 9). The amount of nickel in HPGCM-Ni-900 is 5.95 wt % determined by ICP measurements. Therefore, the saturation magnetizations of nickel can be normalized as 38.7 emu g^{-1}, which is lower than that of the reported bulk metallic Ni (57.6 emu g^{-1}),[30] mainly due to the much smaller Ni nanoparticle size and inclusion of Ni nanoparticles inside the non-magnetic carbon frameworks. The near-zero coercive force and remanence on the magnetization curve indicate the samples exhibit soft ferromagnetic characteristics desirable for the application in adsorption of dyes and separation under an external magnetic field. The inset of Figure 9 shows that HPGCM-Ni-900 materials can be handled under a magnetic field, such as a laboratory magnet.

The magnetic separability of HPGCM-Ni-900 has been tested in MO aqueous solution (Figure 10). Without the magnet, HPGCM-Ni-900 samples disperse in MO solution form a black suspension. Upon placement of a magnet near the glass bottle, the black particles can be attracted to the wall of glass bottle, and the clear solution can be obtained within a few minutes. The colorless solution can be decanted off and the adsorbent can be recovered by washing with ethanol. These results demonstrate that HPGCM-Ni-900 materials can potentially be used as

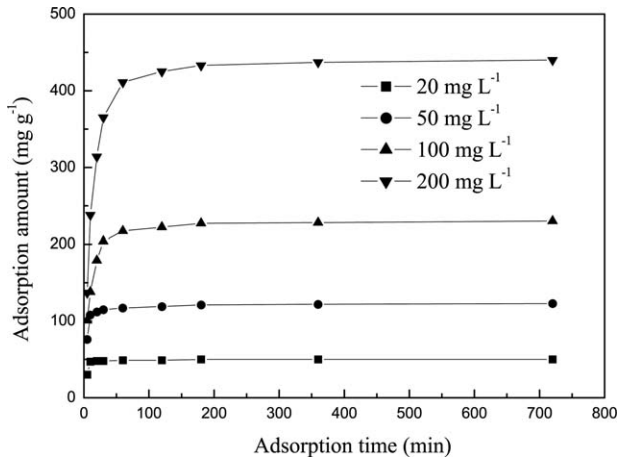

Figure 8. Adsorption of various concentrations of MO (20, 50, 100, and 200 mg L^{-1}) by HPGCM-Ni-900 as a function of contact time.

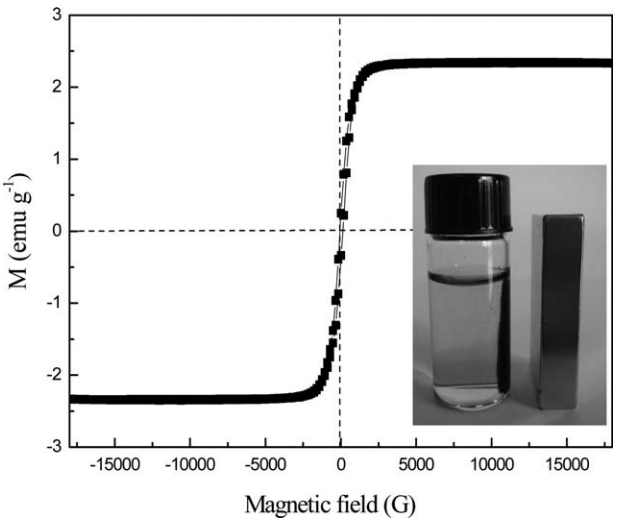

Figure 9. Magnetization curve of HPGCM-Ni-900 recorded at room temperature. Insets are the demonstration of magnetic separation of HPGCM-Ni-900 by applying an external magnet.

Figure 10. Photographs of the initial MO solution (100 mg L^{-1}, left), the solution after mixing with HPGCM-Ni-900 (middle), and the solution after removal of MO dyes by a magnet (right). [Color figure can be viewed in the online issue, which is available at wileyonlinelibrary.com.]

magnetically-separable adsorbents to remove dyes or other large molecules in liquid-phase processes.

CONCLUSIONS

In summary, we have successfully fabricated the HPGCMs containing nickel nanoparticles by using PU foam as macroporous scaffold, triblock copolymer F127 as mesostructure template, diblock copolymer PDMS-PEO as co-template and silica source, resol as carbon precursor, nickel nitrate as graphitic catalyst and magnetic nanoparticles precursor. The synthesized HPGCM-Ni materials possess a hierarchically porous structure with high specific surface area (725 m^2 g^{-1}), large pore size (7.2 nm) and pore volume (0.74 cm^3 g^{-1}), and high saturation magnetization (2.3 emu g^{-1}), which make them ideal candidates for the adsorption of dyes in aqueous solution. This simple and facile fabrication method can open an avenue to the large-scale production of magnetically separable HPGCMs for application in the fields of adsorption and separation.

ACKNOWLEDGMENTS

The authors gratefully acknowledge the financial supports from the Program of Chongqing Municipal Education Commission (KJ121201), the First Excellent Young Teachers Program of Chongqing high school ([2011]65), Chongqing Yongchuan Key Technologies R&D Program (YCSTC, 2011AC4001), Research Program of Chongqing University of Arts and Sciences (Z2011RCYJ04), and the Postdoctoral Research Funding Plan of Jiangsu Province (1302095C), Natural Science Foundation of Jiangsu Province (BK20130617, BK20130619) and National Natural Science Foundation of China (21304018, 21374016).

REFERENCES

1. Yang, W. J.; Wu, D.C.; Fu, R. W. *J. Appl. Polym. Sci.* **2007**, *106*, 2775.
2. Yu, L.; Luo, Y. M. *J. Environ. Chem. Eng.* **2014**, *2*, 220.
3. Figueiredo, J. L.; Sousa, J. P. S.; Orge, C. A.; Pereira, M. F. R.; Órfão, J. J. M. *Adsorption* **2011**, *17*, 431.
4. He, C.; Hu, X. *J. Adsorption* **2012**, *18*, 337.
5. Tian, Y.; Wang X. F.; Pan, Y. F. *J. Hazard. Mater.* **2012**, 213, 361.
6. Dong, Y.; Lin, H. M.; Qu, F. Y. *Chem. Eng. J.* **2012**, 193, 169.
7. Wang, T. B.; Liang, L.; Wang, R. W.; Jiang, Y. Q.; Lin, K. F.; Sun, J. M. *Adsorption* **2012**, *18*, 439.
8. Hao, G. P.; Li, W. C.; Qian, D; Wang, G. H.; Zhang, W. P.; Zhang, T.; Wang, A.Q.; Schüth, F.; Bongard, H. J.; Lu, A. H. *J. Am. Chem. Soc.* **2011**, *133*, 11378.
9. Tao, G. J., Zhang, L. X., Hua, Z. L., Chen, Y., Guo, L. M., Zhang, J. M., Shu, Z., Gao, J. H., Chen, H. R., Wu, W., Liu, Z. W., Shi, J. L. *Carbon* **2014**, *66*, 547.
10. Liu, F. J., Zhang, H.; Zhu, L. F.; Liao, Y. M.; Nawaz, F.; Meng, X. J.; Xiao, F. S. *Adsorption* **2013**, *19*, 39.
11. Lu, A. H.; Li, W. C.; Schmidt, W.; Schuth, F. *Microporous Mesoporous Mater.* **2006**, *95*, 187.
12. Jaroniec, M.; Choma, J.; Gorka, J.; Zawislak, A. *Chem. Mater.* **2007**, *20*, 1069.
13. Álvarez, S.; Fuertes, A. B. *Mater. Lett.* **2007**, *61*, 2378.
14. Xue, C. F.; Tu, B.; Zhao, D. Y. *Nano. Res.* **2009**, *2*, 242.
15. Liang, C.; Dai, S.; Guiochon, G. *Anal. Chem.* **2003**, *75*, 4904.
16. Hu, Y. S.; Adelhelm, P.; Smarsly, B. M.; Hore, S.; Antonietti, M.; Maier, J. *Adv. Funct. Mater.* **2007**, *17*, 1873.
17. Sevilla, M.; Fuertes, A. B. *Carbon* **2013**, *56*, 155.
18. Lei, Z. B.; Xiao, Y.; Dang, L. Q.; Bai, S. Y.; An, L. Z. *Microporous Mesoporous Mater.* **2008**, *109*, 109.
19. Zhao, N. Q.; Wu, S.; He, C. N.; Shi, C. S.; Liu, E. Z.; Du, X. W.; Li, J. *J. Mater. Lett.* **2012**, *87*, 77.
20. Wang, D. W.; Li, F.; Lu, G. Q.; Cheng, H. M. *Carbon* **2008**, *46*, 1593.
21. Huang, C. H.; Doong, R. A.; Gu, D.; Zhao, D. Y. *Carbon* **2011**, *49*, 3055.
22. Meng, Y.; Gu, D.; Zhang, F.; Sh, Y. F.; Yang, H. F.; Li, Z.; Yu, C. Z.; Tu, B.; Zhao, D. Y. *Angew. Chem. Int. Ed.* **2005**, *44*, 7053.
23. Zhao, D. Y.; Feng, J. L.; Huo, Q. S.; Melosh, N.; Fredrickson, G. H.; Chmelka, B. F.; Stucky, G. D. *Science* **1998**, *279*, 548.

24. Yang, H. F.; Yan, Y.; Liu, Y.; Zhang, F. Q.; Zhang, R. Y.; Meng, Y.; Li, M.; Xie, S. H.; Tu, B.; Zhao, D. Y. *J. Phys. Chem. B* **2004**, *108*, 17320.
25. Kiciński, W.; Norek, M.; Bystrzejewski, M. *J. Phys. Chem. Solids* **2013**, *74*, 101.
26. Tang, J.; Wang, T.; Sun, X.; Guo, Y. X.; Xue, H. R.; Guo, H.; Liu, M. Z.; Zhang, X. X.; He, J. P. *Microporous Mesoporous Mater.* **2013**, *177*, 105.
27. Sadezky, A.; Muckenhuber, H.; Grothe, H.; Niessner, R.; Poschl, U. *Carbon* **2005**, *43*, 1731.
28. Ferrari, A. C.; Robertson, *J. Phys. Rev. B* **2000**, *61*, 14095.
29. Hecht, E.; Hoffmann, H. *Langmuir* **1994**, *10*, 86.
30. Si, P. Z.; Zhang, Z. D.; Geng, D. Y.; You, C. Y.; Zhao, X. G.; Zhang, W. S. *Carbon* **2003**, *41*, 247.